TOPICAL REVIEW • OPEN ACCESS

The creation of breast lesion models for mammographic virtual clinical trials: a topical review

To cite this article: Astrid Van Camp et al 2023 Prog. Biomed. Eng. 5 012003

View the article online for updates and enhancements.

You may also like

- Characterization of breast lesions using multi-parametric diffusion MRI and machine learning Rahul Mehta, Yangyang Bu, Zheng Zhong et al.
- Model observer for assessing digital breast tomosynthesis for multi-lesion detection in the presence of anatomical noise Gezheng Wen, Mia K Markey, Tamara Miner Haygood et al.
- Performance evaluation of digital breast tomosynthesis systems: physical methods and experimental data
 N W Marshall and H Bosmans

Progress in Biomedical Engineering



OPEN ACCESS

RECEIVED

31 October 2022

REVISED

17 January 2023

ACCEPTED FOR PUBLICATION

16 March 2023

PUBLISHED

31 March 2023

Original content from this work may be used under the terms of the Attribution 4.0 licence.

Any further distribution of this work must maintain attribution to the author(s) and the title of the work, journal



TOPICAL REVIEW

The creation of breast lesion models for mammographic virtual clinical trials: a topical review

Astrid Van Camp^{1,5,*}, Katrien Houbrechts^{1,5,*}, Lesley Cockmartin², Henry C Woodruff^{3,4}, Philippe Lambin^{3,4}, Nicholas W Marshall^{1,2} and Hilde Bosmans^{1,2}

- 1 Department of Imaging and Pathology, Division of Medical Physics & Quality Assessment, KU Leuven, Herestraat 49, 3000 Leuven, Belgium
- Department of Radiology, UZ Leuven, Herestraat 49, 3000 Leuven, Belgium
- The D-Lab, Department of Precision Medicine, GROW Research Institute, Maastricht University, Maastricht, The Netherlands
- Department of Radiology and Nuclear Medicine, GROW Research Institute, Maastricht University Medical Centre+, Maastricht, The Netherlands
- Both authors contributed equally.
- Authors to whom any correspondence should be addressed.

E-mail: astrid.vancamp@uzleuven.be and katrien.houbrechts@uzleuven.be

Keywords: virtual clinical trials, breast imaging, breast masses, mammography, microcalcifications, lesion models, simulation

Abstract

Simulated breast lesion models, including microcalcification clusters and masses, have been used in several studies. Realistic lesion models are required for virtual clinical trials to be representative of clinical performance. Multiple methods exist to generate breast lesion models with various levels of realism depending on the application. First, lesion models can be obtained using mathematical methods, such as approximating a lesion with 3D geometric shapes or using algorithmic techniques such as iterative processes to grow a lesion. On the other hand, lesion models can be based on patient data. They can be either created starting from characteristics of real lesions or they can be a replica of clinical lesions by segmenting real cancer cases. Next, various approaches exist to embed these lesions into breast structures to create tumour cases. The simplest method, typically used for calcifications, is intensity scaling. Two other common approaches are the hybrid and total simulation method, in which the lesion model is inserted into a real breast image or a 3D breast model, respectively. In addition, artificial intelligence-based approaches can directly grow breast lesions in breast images. This article provides a review of the literature available on the development of lesion models, simulation methods to insert them into background structures and their applications, including optimisation studies, performance evaluation of software and education.

1. Introduction

Virtual clinical trials (VCTs), also known as in silico trials, are valuable for medical imaging system design and performance evaluation. VCTs in medical imaging are based on computer simulations of human anatomy, image acquisition and image interpretation. They allow to study a specific clinical task in a more flexible, cheaper and faster way than real clinical trials, and do not involve exposure risk to the patient (Abadi et al 2020). The ability to synthesise abnormalities enhances the versatility of VCTs and can bring their results closer to clinical practice. Ultimately, scientific studies should prove that VCTs and real clinical trials lead to similar results.

For mammographic systems, such as digital mammography (DM) and digital breast tomosynthesis (DBT), numerous VCTs have been developed to compare the characteristics of imaging systems and investigate their diagnostic performance. For observer studies to be maximally predictive for specific clinical performance questions, realistic or nearly realistic breast lesion models may be useful and even required. Ideally, they cover the notable variations in patient pathology in terms of border characteristics, shape, and contrast. Finding such realistic renditions of diseased conditions and pathologies to represent the clinical variety is a challenge.

Over the years, a number of research groups have employed various approaches to generate computational breast lesions for their VCTs (tables 1 and 2). Lesion models vary from geometrical shapes to models based on segmentations of real lesions in breast images. Multiple methods exist to insert such generated models in either existing or synthetic mammographic images (Marshall and Bosmans 2022). Depending on the task investigated in the VCT, choices must be made regarding the methods used, given their realism, complexity and the available resources.

To the best of our knowledge, this is the first review paper to discuss and compare existing approaches to create breast lesion models in mammographic VCTs. This review first focuses on methods for generating lesions to study breast imaging applications, together with the evaluation of lesion realism. This is followed by a description of how these abnormalities are incorporated into background breast structures. By integrating both microcalcification models and breast mass models, a complete overview is provided for all common breast lesions.

2. Generation of lesion models

Two broad types of abnormalities are detectable on mammograms: calcifications and breast masses. Associated features with these breast lesions include among others skin and nipple retraction, and architectural distortion (American College of Radiology 2013).

Calcifications are small deposits of calcium in the breast that are frequently found on mammographic images. Although many calcifications are benign, they can serve as a marker of an underlying malignant process. Therefore, their detection is of utmost importance. Different types of calcifications have been described by Le Gal *et al* (1984) and are listed in the breast imaging reporting and data system (BI-RADS) lexicon (American College of Radiology 2013). Whereas benign calcifications tend to be larger, rounder and smoother, malignant calcifications often have a more irregular or punctate shape (Burnside *et al* 2007). A cluster consists of multiple microcalcifications, usually smaller than 1 mm in diameter, located in a small region. Clusters with linear or pleomorphic microcalcifications are clinically more suspicious for malignancy (Bent *et al* 2010). In clinical practice, it is important to distinguish between benign and malignant clusters. Therefore, imaging modalities should be able to visualise both types accurately.

Masses occupy a larger region within the breast and contain a collection of cancer cells intermingled with normal breast tissue or necrotic tissue. Masses vary in density, shape (round, oval, irregular) and margin (circumscribed, obscured, microlobulated, indistinct, spiculated) (American College of Radiology 2013). The contour is the most discriminating morphological criterion between benign and malignant masses. Benign masses are often well-defined, circumscribed and roughly spherical, whereas dense, irregularly shaped tumours with ambiguous edges are usually categorised as malignant (duCret 1997).

Architectural distortions of breast tissue represent the third most common means by which malignancy can be detected. It must be noted that there are a number of benign causes of architectural distortions, including radial scars and fat necrosis, but these have not yet been taken up in VCTs (Gaur *et al* 2013). Their prevalence on mammography is low compared with calcifications or visible masses. However, inclusion of such features would ultimately increase the realism of simulated breast cancer cases and may be important when accounting for false positive generating signals. Skin and nipple retraction also indicate the possibility of malignancy, even though they are not the ultimate target that radiologists are looking for. To our knowledge, no systematic attempt has been made to simulate factors causing distortions and we consider these features outside the scope of this paper.

We focus on the means of generating breast lesions, first discussing microcalcification clusters followed by breast masses. Both lesions are considered in order of increasing complexity, from the simplest geometrical models to complex structures based on the properties of real breast lesions.

2.1. Microcalcification clusters

2.1.1. Microcalcification models based on mathematical models

2.1.1.1. Geometric shapes

In its most simple form, a calcification is often modelled as a sphere or ellipsoid, as shown in figure 1(a). Bliznakova *et al* (2003, 2006) simulated six microcalcifications ranging from 0.1 to 1.0 mm as ellipsoids of calcium carbonate (CaCO₃) and inserted them into their three-dimensional (3D) uncompressed breast model. Similarly, Makeev *et al* (2021) introduced ellipsoids of calcium oxalate (CaOx) and calcium hydroxyapatite (CaHa) into the central slice of a digital phantom. Sizes could vary between 0.2 and 1 mm, with voxels at the edges of the ellipsoids removed randomly to create more irregular calcification shapes. Clusters were constrained to a size of 6 mm with 5–15 individual microcalcifications. Van Camp *et al* (2022) altered the edges of initial spheres by adding noise, followed by thresholding the resulting intensities in an attempt to create realistic, benign microcalcifications. Figure 1(b) shows such microcalcifications inserted in

 Table 1. Overview of breast lesion models based on mathematical methods.

Cal	Calcification clusters			Breast masses	
		Lesions based	Lesions based on mathematical models		
		Ge	Geometric shapes		
Bliznakova <i>et al</i> (2003), (2006), Näppi <i>et al</i> (2001)	Spheres and ellipsoids	Benign	Bakic et al (2018a)	Spheres and oblate spheroids	Benign
Makeev et al 2021	Ellipsoids with a fraction of voxels removed	Benign & malignant	Mainprize <i>et al</i> (2016), Lago <i>et al</i> (2018)	3D Gaussian blobs	Diffuse-edged mass
Van Camp et al (2022), Li et al (2018)	Spheres with altered edges by added noise	Benign	Bakic et al (2018b), Lago et al (2018)	(non-)concentric shells with different attenuation properties	Benign & irregular
Reiser and Nishikawa (2006)	2D models of ellipse, disk and star shape	Benign & malignant	Timberg et al (2010)	Manually drawn 2D contours extended to ellipsoidal shapes	Irregular
Kallergi <i>et al</i> (1998)	2D manually drawn contours based on BI-RADS description	Benign & malignant			
		Algor	Algorithmic techniques		
Bliznakova <i>et al</i> (2003), Ruschin <i>et al</i> (2005), Näppi <i>et al</i> (2001)	Random walk algorithm	Malignant	Chen <i>et al</i> (2011)	Stochastic growth model: glandular tissue reduces towards outer ellipsoidal shells	Irregular
Ruschin et al (2005)	Wireframe models	Malignant (elongated)	Gong et al (2006)	Sphere with spicules grown with stochastic growth method	Irregular
Bliznakova et al (2003)	Combination of cylinders	Malignant (elongated)	Sánchez De La Rosa (2019)	Consolidation of ellipsoids as basic shape; spicules grown using random walk algorithm	Irregular
Ho et al (2010)	Epipolar curves	Malignant	Hintsala et al (2009), Rashidnasab et al (2013b), Bliznakova et al (2019)	Random walk algorithm	Irregular
			Rashidnasab <i>et al</i> (2013), Rashidnasab <i>et al</i> (2013b), Hadjipanteli <i>et al</i> (2019)	Diffusion limited aggregation (DLA)	Irregular
			De Sisternes et al (2015)	Low and high frequency modifications to Gaussian random sphere; spicules grown using iterative branching algorithm	Irregular

Table 2. Overview of breast lesion models based on patient data and tumour growth models.

	Calcification clusters			Breast masses	
		Lesions based	Lesions based on patient data		
		Segmentation in m	Segmentation in mammographic image		
Yam et al (2001)	Automatic segmentation from 2D mammograms; calcifications are approximated with ellipsoids	Benign & malignant	Das et al (2009)	Concatenation of manually drawn 2D objects based on histopathological sections	Irregular
Daul et al (2005), Tiedeu et al (2005)	Automatic segmentation from stereotactic 2D mammographic images	Benign & malignant	Shaheen et al (2014)	Segmentation from breast MRI images; spicules grown using iterative branching algorithm	Irregular
Lado <i>et al</i> (1997), Suryanarayanan <i>et al</i> (2005), Saunders <i>et al</i> (2006), Vivona <i>et al</i> (2014)	Automatic segmentation from 2D mammograms	Benign & malignant	Bliznakova <i>et al</i> (2019), Dukov <i>et al</i> (2019)	Segmentation from DBT and breast CT images	Irregular
From	From images of biopsied clusters		Stati	Statistical models based on characteristics of real lesion	u
Carton et al (2003)	Automatic segmentation from biopsied clusters imaged with film-screen; concentric rings added to calcifications	Malignant	Elangovan et al (2016b)	Spicule skeleton based on patient data attached to DLA mass	Irregular
Zanca et al (2008, 2009), Warren et al (2012)	Automatic segmentation from DM images of biopsied clusters	Malignant	Saunders et al (2006)	Mass model based on lesion shape, contrast and edge properties of real lesions	Benign & irregular
Shaheen <i>et al</i> (2011), Van Camp <i>et al</i> (2022)	Automatic segmentation from 3D images of biopsied clusters obtained with a cone-beam micro-CT scanner	Benign & malignant	Berks et al (2008, 2010)	Combination of mass appearance model (shape, size, texture) and mass background appearance model (spicules, distortions)	Irregular
		Tumour gr	Tumour growth models		
Plourde <i>et al</i> (2016)	Tumour growth model incorporating background pressure	Benign & malignant	Sengupta et al (2021)	Tumour growth model incorporating local anatomy	Benign & irregular
	,		Tomic <i>et al</i> (2021)	Growth of spheres based on clinical data to simulate multiple time points	Benign

Figure 1. Examples of geometric shaped calcifications. (a) Round and ovoid calcifications simulated as spheres and ellipsoids respectively. Reproduced from (Bliznakova *et al* 2003). © IOP Publishing Ltd. All rights reserved. (b) A benign cluster consisting of spheres altered by adding noise. Reproduced with permission from (Van Camp *et al* 2022). (c) Disk, ellipse and star shaped calcifications. (Reiser and Nishikawa 2006) John © 2006 American Association of Physicists in Medicine. (d) Binary image of pleomorphic calcifications based on manually drawn contours. Reprinted from (Kallergi *et al* 1998), Copyright (1998), with permission from Elsevier.

a mammographic image. Similarly, Li *et al* (2018) introduced irregularities by modifying ellipsoidal surface meshes with stochastic Perlin noise.

Based on the findings of anatomical properties, Näppi $et\,al\,(2001)$ also found ellipsoids to be representative of calcifications. They distinguished three principal calcification shapes visualised in figure 2(a): ovoid, irregular and elongated structures with the ovoid shape consisting of an ellipsoid of which the axis ratio could be varied. Creating models with a linear attenuation coefficient ranging between calcium and fatty tissue ensured a variety of calcification types with different densities. Reiser and Nishikawa (2006) discussed the creation of three different shapes as well, i.e. ellipse, disk and star shape, but limited them however to a two-dimensional (2D) model. All three shapes are modelled with a standard axis ratio (figure 1(c)). Validation experiments were conducted to investigate how readers could distinguish between the three shapes.

Also using 2D models, Kallergi *et al* (1998) manually drew microcalcification contours based on the BI-RADS morphological description (D'Orsi and Kopans 1993). Different groups of calcifications, both benign and malignant, were created. Unlike the standardised ellipsoids, this method could be applied to create a larger ensemble of unique calcifications, ranging from round benign structures to fine linear malignant structures, as shown in figure 1(d).

2.1.1.2. Algorithmic techniques

To generate more complex shapes, algorithmic techniques have been applied.

To create a large set of (irregularly shaped) microcalcifications, Bliznakova *et al* (2003) and Ruschin *et al* (2005) used a random walk algorithm. Starting from a central pixel, each iteration extended the calcification volume to a randomly selected new location by choosing a neighbouring pixel. A new branch could then be created with 5% probability. After a predetermined number of iterations or when one branch reached a predefined border, the random walk iterative process ended. Further, erosion and dilation operations ensured a continuous yet blurry border. Afterwards, the microcalcifications were scaled down in size such that the diameters were within 0.1–1.5 mm. Clusters were then created by combining microcalcifications with user-defined parameters such as the number of calcifications, cluster density and height-to-width ratio. For each added microcalcification, the location, orientation and normalised pixel value being between 0.1 and 1.0, were chosen randomly.

In contrast to the method for generating ovoid structures, Näppi *et al* (2001) used a random walk model to simulate irregular microcalcification shapes. As for Ruschin *et al* (2005), the algorithm ended when a border was reached, and a final dilation step ensured that the method created irregular microcalcification clusters with a powder-like appearance, as shown at the top of figure 2(a) and in figure 2(b). Wireframe models were used in order to create elongated calcifications. An initial line defining the length of the calcification was altered using a random midpoint displacement algorithm. This fractal method recursively splits a polyline at the midpoint of each line and displaces these sections to obtain a new, more complex polyline. The simulated calcification then resided within a specified radius of the wireframe described by the final polyline. Similarly, Bliznakova *et al* (2003) modelled elongated microcalcifications by arranging cylinders with specified heights and radii.

Some studies modelled clusters in DBT as an ellipsoidal envelope (Ho *et al* 2010). Here the radii of the ellipsoids could be varied to create different types of clusters. For a linear shape, one of the radii was large compared to the others. Microcalcifications were then generated within the envelope by defining an epipolar curve for each calcification. Such a curve defines the 2D projections of a 3D object in the DBT image. The 3D model is constructed by finding the intersection points of curves joining the 2D pixels of microcalcifications.

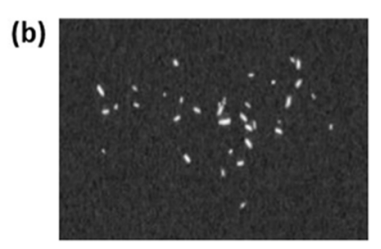
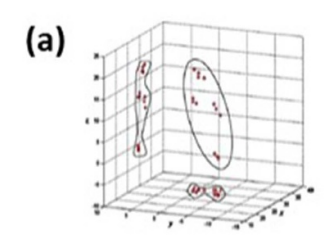


Figure 2. Examples of calcifications created with algorithmic techniques. (a) Examples of irregular (top), ovoid (middle) and elongated (bottom) calcifications. Reprinted from (Näppi *et al* 2001), Copyright (2001), with permission from Elsevier. (b) A simulated microcalcification cluster based on a random walk model. (Ruschin *et al* 2007) John © 2007 American Association of Physicists in Medicine.



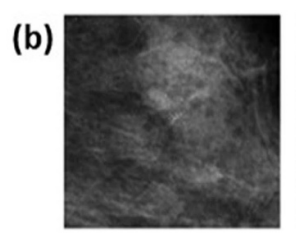




Figure 3. Microcalcification clusters obtained from segmentations in mammographic images. (a) 3D model of a cluster reconstructed and matched from its two views. Reprinted from (Tiedeu *et al* 2005), Copyright (2005), with permission from Elsevier. (b) Simulated (left) and real (right) microcalcification cluster. Reprinted from Saunders *et al* (2006). Copyright (2006), with permission from Elsevier.

2.1.2. Microcalcification models based on patient data

2.1.2.1. Segmentation in mammographic images

Whereas the methods discussed above create new calcifications from scratch, much research has focused on the use of real clusters segmented from patient images, to generate a dataset of realistic calcifications.

In order to extract calcifications from images, Yam *et al* (2001) defined the ratio of the volume of interesting or non-fat tissue to the estimated volume of a blob in the breast. Given that calcifications have a high x-ray attenuation coefficient compared to soft tissue, the calcification attenuation is comparable to that of much thicker tissue. A threshold was applied to the ratio to detect calcifications. The 3D volume of each calcification was then approximated using an ellipsoid. After performing this step in two views, the calcifications were matched to reconstruct clusters in 3D.

While Yam et al (2001) used craniocaudal and mediolateral oblique views to reconstruct clusters in 3D, Daul et al and Tiedeu et al (2005, 2005) extracted cluster models from images obtained with a stereotactic mammographic unit. Because the cluster was indicated in two views, the 3D position could be found at the intersection of the 3D trajectories (figure 3(a)). A method proposed by Chan et al (1998) was then adapted, namely applying filters to enhance the contrast between microcalcifications and background. Possible calcifications were segmented from the background tissue and then computed features of the possible calcifications were used to eliminate false positives.

While these models have focused on synthesizing 3D clusters from multiple 2D images, most research regarding microcalcifications only considers the 2D projection in mammographic images. The disadvantage of 2D models is that less features of real clusters could be calculated and considered when generating realistic simulations.

Such a method is discussed in Lado et~al~(1997), where a wavelet transform was used to segment microcalcifications from real DM images. Regions of interest (ROIs) containing a microcalcification cluster were used to create reconstructed images. After a wavelet transform, high-frequency components were enhanced by decomposition up to the third level, which removed the low-frequency background structures. A final histogram threshold was chosen to obtain a high sensitivity for seed points of microcalcifications while limiting the number of false positives. A region growing method with a grey level threshold was then applied to detect the complete microcalcification using spatially connected pixels. Features such as mean contrast, average grey level, size and number of microcalcifications per cluster were then extracted from the real, segmented microcalcifications. When simulating new clusters in images, these features were used to constrain the properties of the clusters. In an observer study, the area under the receiver operating characteristic (ROC) curve (AUC) of 0.54 ± 0.03 denoted the realism of the simulated microcalcifications.

Figure 4. Models of segmented microcalcifications. (a) Calcification with two central parts and four concentric rings. (Carton *et al* 2003) John Wiley & Sons. [© 2003 American Association of Physicists in Medicine]. (b) 3D model of a microcalcification cluster obtained from an imaged biopsied specimen. (Shaheen *et al* 2011) John Wiley & Sons. [© 2011 American Association of Physicists in Medicine].

To obtain realistic microcalcification clusters, Suryanarayanan *et al* (2005) applied filtering to suppress microcalcifications in mammographic images with a single cluster. The lesions were segmented by subtracting the filtered image from the original image to remove undesirable background structures. Based on the location and intensity of the resulting extracted microcalcification cluster, plausible locations for new microcalcifications were chosen by selecting pixel intensities within a certain range. Pixels with amplitudes and shapes in the same range as real calcifications were inserted in mammographic images and grouped to create new microcalcifications resulting in a hybrid cluster of real and simulated microcalcifications.

Saunders *et al* (2006) segmented microcalcifications from ROIs by thresholding after converting the pixel values to optical density. Additional manual inspection ensured that all calcifications were included, and the properties of these microcalcifications were later used to simulate new clusters. It was assumed that microcalcifications in a cluster resided either within an ellipse for the clustered pleomorphic case or were distributed along lines and branches for the fine linear branching case. A single microcalcification was then modelled from a line, with thickening and erosion to ensure realistic edges. In an observer study, no significant difference was noted in realism scores for the appearance of simulated and real microcalcifications, examples of which are shown in figure 3(b).

Vivona *et al* (2014) first applied edge detection to extract ROIs from an image. High pass filtering was then used to suppress the background, and a spatial filter designed to detect microcalcifications was applied. A physician then identified which of the proposed ROIs actually contained a cluster and stored the real clusters in a database. When clusters were simulated in a new breast, they consisted of microcalcifications taken from the database of real microcalcification clusters where relative angles and distances between microcalcifications were maintained. These simulated clusters were used to test a Fuzzy C-means clustering algorithm.

2.1.2.2. From images of biopsied clusters

To obtain models of real microcalcifications, Carton et al (2003) imaged biopsied clusters with a storage phosphor plate system in DM magnification view to obtain a high resolution image. After linearization of the raw ('for processing') images, the pixel value intensities corresponded linearly to the x-ray exposure. The lowest x-ray transmission denoted the thickest part of the microcalcification that was then defined as the 'core'. Concentric ring-like shapes, composed of pixel values with similar grey values, were then constructed around this central core and further characterised from the extracted features of calcifications. As shown in figure 4(a), the visualised microcalcification has up to four concentric rings. New microcalcifications could then be simulated by adjusting the ideal calcification templates to the mean energy of the x-ray beam and the resolution of the detector. In a two-alternative forced choice study, there was no perceived difference between simulated and real lesions. Similarly, Zanca et al (2008, 2009) obtained DM images of biopsied cluster specimens superposed on polymethyl methacrylate. Individual microcalcifications were then digitally extracted. Normalizing the pixel values to the average pixel value of the background produced a template of the cluster. These templates were adjusted to simulate the desired acquisition conditions on a mammography system as in Carton et al (2003) or to specific set values. These simulated clusters could not be distinguished from real clusters, which was proven in an observer study by radiologists. In the same manner, Warren et al (2012) imaged biopsied clusters and created templates too. The microcalcifications within each cluster were rearranged to increase the number of available clusters. Simulations in DM images by Zanca et al (2008) and Warren et al (2012) are shown in figure 5.

In the work of Shaheen *et al* (2011), biopsied clusters were again the data source, but were now imaged with a cone-beam micro-CT scanner. Microcalcifications were segmented from 3D images using Sobel edge detection, morphological operations and median filters. Rotation was used to increase the initial set of

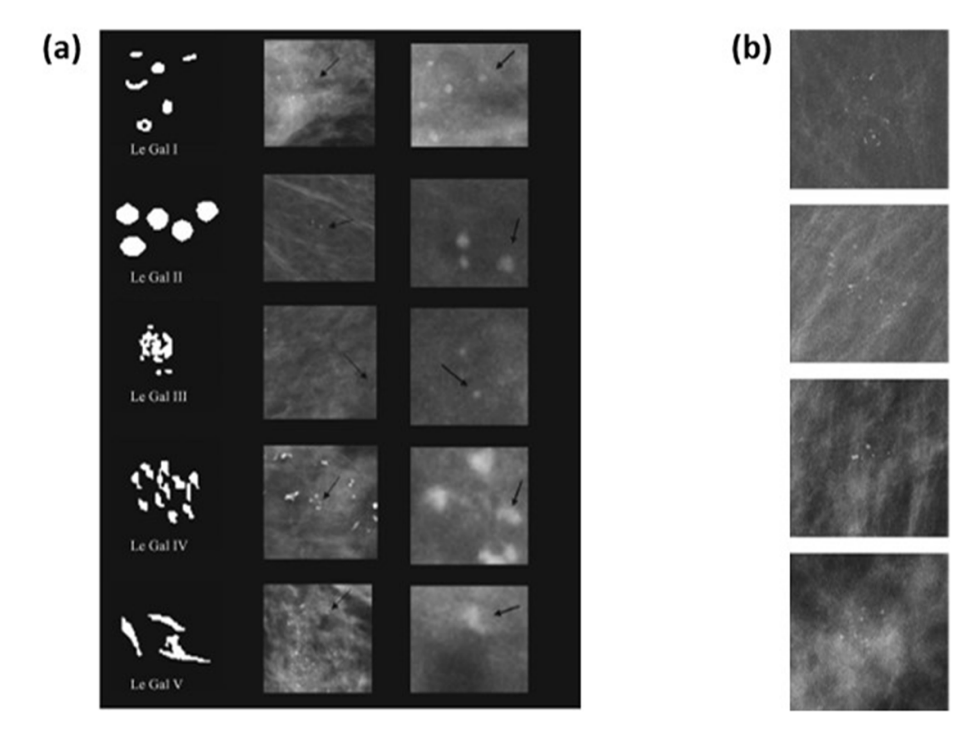


Figure 5. Examples of microcalcification clusters. (a) Simulated clusters (indicated by the arrow) together with their magnified view (third column) and their corresponding Le Gal type on the left. (Zanca *et al* 2008) John Wiley & Sons. [◎ 2008 American Association of Physicists in Medicine]. (b) Clusters inserted in breast images with different glandularities (fatty on top, glandular at the bottom). (Warren *et al* 2012) John Wiley & Sons. [◎ 2012 American Association of Physicists in Medicine].

clusters if 2D projections were found to be sufficiently different, resulting in a database of 54 3D microcalcification cluster models, one of which is shown in figure 4(b). From such 3D models, 2D projected templates could be created for use in image simulations. The study of Hadjipanteli *et al* (2017) created new simulated clusters starting from a single microcalcification extracted from the database of Shaheen *et al* (2011). This microcalcification was resized and recombined five times to create a cluster which was then rotated. The same database formed the basis of the study by Van Camp *et al* (2022) where microcalcifications were recombined to create new malignant clusters. A large set of clusters could be created by applying random choices on the rotation and location of microcalcifications while still considering the properties of real clusters. In a validation study to distinguish real from simulated clusters, an average AUC of 0.53 was obtained.

2.1.3. Growth within mammographic images

In order to simulate the growth of microcalcification clusters, Plourde *et al* (2016) started from a mammographic background with normalised pixel intensities. The growth process was based on tumour pressure, which defined the force per unit area used to control lesion growth. Different growth rules were applied for benign and malignant calcifications formed from hydroxyapatite and calcium oxide respectively. Growth was tempered by the resistance of the background tissue and 3D factors represented by a separate model parameter. Starting from seed points, a calcification thus grew when the difference between the tumour pressure of the surrounding pixels and the tissue value at the given position was larger than a constraining factor.

2.2. Breast masses

2.2.1. Mass models based on mathematical models

2.2.1.1. Geometric shapes

Circumscribed masses, where the contour is clearly defined at the larger part of their surface, and which are usually associated with benign breast findings, can be approximated with geometric shapes (American College of Radiology 2013).

In their simplest form, mass lesions can be represented by solid spheres and oblate spheroids with the contrast of the masses controlled by varying the thickness of the ellipsoids (Bakic *et al* 2018a). Some of these lesions are shown in figure 6(a).

Figure 6. Examples of geometric shaped mass lesions. (a) Solid ellipsoids (oblate spheroids) used for simulating breast masses. Reproduced with permission from (Bakic *et al* 2018a). (b) 3D Gaussian blob to approximate a diffuse-edged mass. (c) Models of one spherical lesion and two non-spheroidal circumscribed lesions consisting of (non-)concentric shells composed of different simulated materials. Reproduced with permission from (Bakic *et al* 2018b).

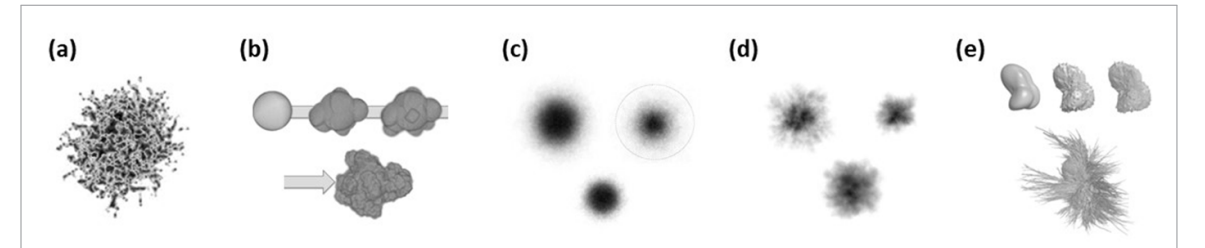


Figure 7. Examples of irregularly shaped masses created with mathematical models. (a) A mass with a stochastic stellate pattern composed of a dense centre and a gradually fading boundary. Reprinted from (Chen *et al* 2011), Copyright (2011), with permission from Elsevier. (b) An iterative process to generate irregular shapes. Reproduced with permission from (Sánchez De La Rosa 2019). (c) Projections of 3D masses created with a random walk algorithm. Reproduced from (Rashidnasab *et al* 2013b). © IOP Publishing Ltd. All rights reserved. (d) 2D projections of DLA masses. Reproduced from (Rashidnasab *et al* 2013b). © IOP Publishing Ltd. All rights reserved. (e) Process of generating a simulated mass model starting from a stochastic Gaussian random sphere model to simulate a central tumour and a fractal branching algorithm to model spicules. Reproduced from (De Sisternes *et al* 2015). CC BY 3.0.

To model a diffuse-edged mass, a number of studies have used a 3D Gaussian blob (figure 6(b)) as an approximation (Mainprize *et al* 2016, Lago *et al* 2018). To ensure that the lesion blends into the surrounding healthy tissue, Bakic *et al* (2018b) and Lago *et al* (2018) built up lesions from multiple shells with different attenuation properties. Figure 6(c) shows how concentric shells were used to model spherical breast lesions, while non-spheroidal circumscribed lesions with a more clinically plausible appearance were generated using a set of non-concentric ellipsoids.

Instead of starting with a geometric shape, Timberg *et al* (2010) started by defining the shape of the lesion in the central 2D plane. Planes above and below were simulated by decreasing the dimensions of the central plane as if the object was an ellipsoid.

2.2.1.2. Irregularly shaped masses

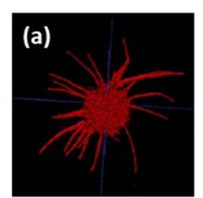
A greater variety of mathematical methods has been used to create irregularly shaped lesions, which are consistent with a greater likelihood of malignancy (American College of Radiology 2013).

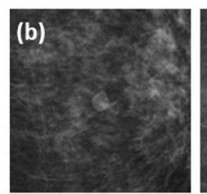
The work of Chen *et al* (2011) implemented a simple stochastic growth model. The percentage of glandular tissue within each ellipsoidal shell was reduced towards the edge of the lesion. This resulted in a lesion with a dense centre and gradually fading boundaries (figure 7(a)).

In a study by Gong *et al* (2006), breast lesion simulation began with a sphere as the basic shape. Spicules were then grown in a randomly chosen direction using a stochastic growth method to improve the realism of the lesion appearance.

Figure 7(b) depicts an analogous method developed by Sánchez De La Rosa (2019) to generate 3D lesions for contrast-enhanced mammography. As basic shape, a spherical or ellipsoidal structure was first created. The surface was further deformed by uniformly distributing seed points on the surface, which formed the centres of new spheres or ellipsoids. This procedure was repeated several times to generate more complex lobulated masses. If a spiculated margin was desired, multiple spicules were grown from the surface using a random walk algorithm. In this model, each spicule is a concatenation of overlapping spherical objects.

As was the case for microcalcifications, the nearest neighbour random walk algorithm can also be used to produce irregular boundaries commonly seen on malignant masses. Similarly, each new random walk was initiated from the central voxel of a 3D binary matrix. At each step of the random walk, an adjacent voxel was randomly selected and assigned as part of the mass. The two key parameters used in this approach are the







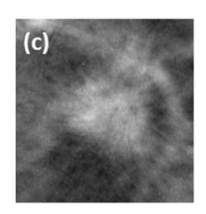


Figure 8. Examples of lesion models based on characteristics of real lesions. (a) Spiculated mass created by adding synthetic spicules extracted from patient images to a DLA mass. Reproduced with permission from (Elangovan *et al* 2016b). (b) Example of a benign (left) and malignant (right) simulated mass with their characteristics tuned to real lesions. Reprinted from Saunders *et al* (2006). Copyright (2006), with permission from Elsevier. (c) Synthetic malignant mass as a result of a mass appearance model and mass background appearance model. Reproduced with permission from (Berks and Barbosa da Silva *et al* 2010).

number of steps in each random walk, which controls the size of the simulated mass, and the number of iterations in the random walk used to build the mass, which controls the texture/density. Morphological image processing, such as averaging, dilation and erosion, was used to smooth the simulated mass (Hintsala *et al* 2009, Rashidnasab *et al* 2013b, Bliznakova *et al* 2019) resulting in masses as shown in figure 7(c).

An alternative approach to simulate mass lesions is the use of diffusion limited aggregation (DLA), a type of fractal growth. Randomly moving particles are launched from concentric spheres around the mass centre and aggregate on the central core as they reach adjacent voxels lining the centre. Using this method, asymmetric breast lesions with a porous volumetric appearance, such as those in figure 7(d), can be simulated. User-defined growth prescriptions that control the size, texture and density of the masses, allow a wide variation in the appearance of the simulated masses (Rashidnasab *et al* 2013a, 2013b, Hadjipanteli *et al* 2019). These masses are currently used in the OPTIMAM platform (Elangovan *et al* 2018).

The appearance of DLA lesions has been validated for realism by means of observer studies in DM (Rashidnasab *et al* 2013b) and DBT modalities (Rashidnasab *et al* 2013a). The insertion of these masses in DM images resulted in higher realism scores than insertion into DBT images. The DLA masses were also compared to masses developed using random walk methods. Observers had greater difficulty distinguishing between real or simulated DLA masses compared to random walk generated masses, and gave higher realism scores to DLA masses (AUC of 0.55 for DLA masses, AUC of 0.60 for random walk masses) (Rashidnasab *et al* 2013b).

The work of De Sisternes *et al* (2015) described an algorithm to create detailed 3D non-spiculated and spiculated breast masses controlled by user-defined parameters. This allows a large family of masses having particular characteristics. Low and high frequency modifications were introduced to a central lesion produced with a Gaussian random sphere technique. Spiculated masses could be generated if desired, with spiculation structures added to the central mass using an iterative branching algorithm. Figure 7(e) illustrates this algorithm. Mass realism was evaluated when inserted into clinical DM images, with an AUC of 0.544 for non-spiculated tumours and 0.588 for spiculated masses. This mass generation algorithm was used in the VICTRE trial (Badano *et al* 2018) and applied by Shaheen *et al* (2014).

2.2.2. Mass models based on patient data

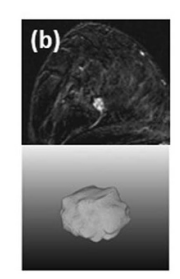
Rather than relying on mathematical functions, one can also start mass generation from patient data. This approach guarantees a high degree of realism of the created models, i.e. conformity to real anatomical structures.

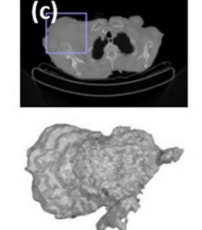
2.2.2.1. Statistical models based on characteristics of real lesions

One approach is to parameterise breast lesions from patient data. The features extracted from real masses are then used to generate digital models.

Elangovan *et al* (2016b) extended the DLA model to simulate spiculated lesions by using features, in terms of spicule length, width, curvature and distribution, extracted from patient DBT images containing spiculated lesions. These features were used as a guide to simulate realistic spicules which were then attached to the surface of a DLA mass resulting in models as shown in figure 8(a). In a validation study, a radiologist rated 60% of the simulated lesions in DM and 50% of the simulated lesions in DBT as realistic.

For the feature extraction, Saunders *et al* (2006) considered two types of typically benign masses (oval circumscribed and oval obscured masses) and two types of typically malignant masses (irregular ill-defined and irregular spiculated masses). For each mass type, three physical characteristics were measured from breast masses in mammographic images: (1) lesion shape using a Laplacian of Gaussian edge detection method, (2) mass contrast using an edge gradient profile, and (3) edge properties using a border deviation profile. Next, a simulation procedure was developed to generate masses that matched the measured data from





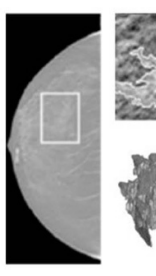


Figure 9. Examples of lesion models created by segmenting patient images. (a) Slices of a 3D simulated lesion based on a histopathological section of an invasive ductal carcinoma. (Das *et al* 2009) John Wiley & Sons. [© 2009 American Association of Physicists in Medicine]. (b) 3D voxelised model of a lesion extracted from breast MRI. (Shaheen *et al* 2014) John Wiley & Sons. [© 2014 American Association of Physicists in Medicine]. (c) Breast lesion models created from segmentation of patient CT images (left) and tomosynthesis (right). Reprinted from (Bliznakova *et al* 2019), Copyright (2019), with permission from Elsevier. Reprinted from (Dukov *et al* 2019), Copyright (2019), with permission from Elsevier.

real lesions. Figure 8(b) shows simulated lesions which observers generally rated to have a similarly realistic appearance to real lesions in DM, with an AUC of 0.68 for benign masses and 0.65 for malignant masses.

To describe the appearance of a set of real malignant masses, Berks *et al* (2008, 2010) constructed two statistical models. The mass appearance model encapsulated the variation in shape, size and texture of the lesion, while the mass background appearance model accounted for how the surrounding structures would be altered by the presence of a mass. The latter was done by modelling the distortion, but also included any spicules associated with the mass. A combined model of appearance was used to synthesise malignant masses by randomly sampling from the model distribution which resulted in a mass as shown in figure 8(c). These masses were evaluated in a DM image dataset using an ROC study, with an AUC of 0.70.

2.2.2.2. Segmentation from breast images

Another approach is to use clinical images from 3D breast imaging modalities, such as DBT, breast computed tomography (CT) and breast magnetic resonance imaging (MRI), to extract full 3D breast lesion shapes instead of extracting only common lesion features.

Using the appearance of malignant masses in CT specimen reconstructions and histopathological sections as an example, Das *et al* (2009) manually defined spiculated 2D objects (figure 9(a)). In order to obtain a 3D mass model with spiculated borders, these 2D objects were connected to create a non-uniform rational B-spline surface.

In the study by Shaheen *et al* (2014), benign and malignant masses were manually segmented from breast MRI images to generate non-spiculated 3D mass models, as shown in figure 9(b). Spicules were not captured in the segmentation procedure because of the low spatial resolution of MRI data. An iterative branching algorithm was used to add spicules of various lengths and diameters to the central mass. In an observer study, radiologists scored the realism of the simulated masses, with an AUC of 0.58 in DM and 0.67 in DBT.

A semi-automatic segmentation algorithm using region growing to segment breast lesions from patient DBT images, as well as from breast cadavers and whole-body CT scans, has been described by Bliznakova *et al* (2019) and Dukov *et al* (2019). The spatial resolution of the obtained 3D segmented models in figure 9(c) is intrinsic to the imaging modality.

2.2.3. Tumour growth model

A difficulty, especially for mass lesions, is the insertion or integration of the tumour model within normal breast background structures. An approach to overcome or limit these difficulties is described by Sengupta *et al* (2021). Breast tumour growth was modelled by considering the local anatomy which exerts pressure and thus influences the shape of the lesion. Two types of non-spiculated lesion models were developed, one using random growth (disc-like lesions) and an alternative using *in-situ* growth.

Tomic *et al* (2021) modelled tumour growth in computer breast phantoms to simulate multiple screening rounds with varying time intervals. The initial tumours were approximated by spheres and grown exponentially based upon clinical tumour volume doubling time values.

3. Lesion insertion and image simulation

Once models of microcalcification clusters and breast masses have been created, the next step is inclusion in a projection image or phantom model as part of the VCT workflow. Depending on the lesion type and occurrence, specific research questions can be addressed by the VCT. Breast lesion models can be introduced

into parenchymal background structures in multiple ways. In the simplest method, mainly used for calcifications, the simulated lesion is combined with a mammographic image and its intensity is scaled to create realistic contrast levels relative to the background. A number of studies consider detailed system modelling where many parameters are considered. There are two general approaches (Marshall and Bosmans 2022). The first is a hybrid simulation method, in which a lesion template is produced using x-ray projection ray tracing and inserted into a real breast image. The alternative is termed 'total simulation', where the lesion is inserted into a 3D breast model, and a simulated image of this breast model with lesion is generated using the VCT imaging pipeline. In addition, an artificial intelligence-based approach can be considered where breast lesions are grown directly in the breast image based on characteristics the model learned from real breast cancer image data. This method does not consist of the two-step approach, where first a separate lesion model is created followed by insertion in a breast image or breast phantom, so no virtual imaging step is required.

3.1. Intensity scaling

Instead of performing a complex simulation, many methods perform simple mathematical computations to combine the simulated lesion and the background tissue. The intensity values of the surrounding tissue or of other real lesions are then considered to scale the intensity of the simulated lesions to obtain a realistic contrast

In a study by Suryanarayanan *et al* (2005), simulated microcalcifications were added to the vicinity of real microcalcifications used for the models. The pixel intensity was measured and found to be within the range of pixel intensities of real microcalcifications. Vivona *et al* (2014) considered the average intensity of a cluster relative to the intensity of the parenchyma as well.

Cluster insertion in the work of Lado *et al* (1997) started with manually positioning the cluster centre in the breast image. The positions of the microcalcifications were then determined based on their locations in the cluster relative to the centre. The pixel intensity of each microcalcification was determined by the average grey level value of the fifth concentric ring in the tissue surrounding the border of the microcalcification. The grey levels of each concentric ring of the microcalcification were then scaled based on this value. Finally, low pass filtering resulted in a uniform distribution between the simulated lesion model and the surrounding tissue.

Reiser and Nishikawa (2006) created mammographic background images from a computer-generated white noise or patient data. The lesion models were 2D and therefore x-ray projection was not performed. The lesion template intensity was scaled to the background with a multiplication factor that resulted in a human reader detection performance of 75%–90% of the cases.

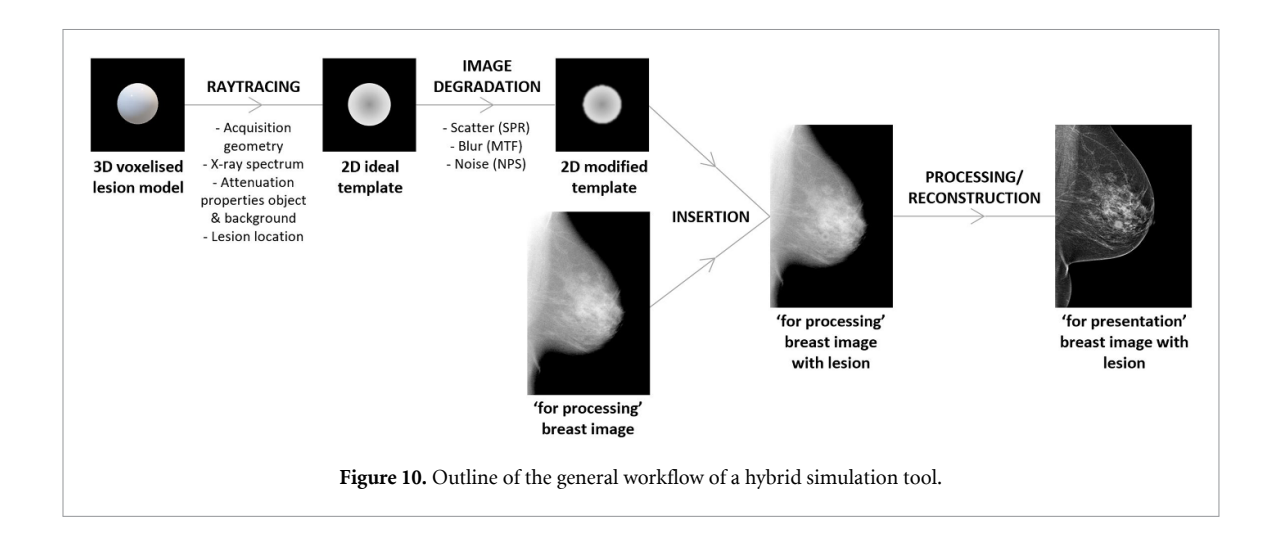
Instead of automatically computing the pixel intensity, Ruschin *et al* (2005) allowed the user to adjust the contrast of the lesion themselves. Radiologists provided feedback regarding which contrast values were acceptable. This was done for a template of the lesion model of normalised intensity values ranging from 0 to 1, where 1 represented the maximal intensity added to the mammographic image.

Saunders *et al* (2006) used this intensity scaling approach to add both microcalcifications and masses to a normal background captured with screen-film images. The contrast of the lesions was estimated by examining the contrast of comparable lesions imaged with identical system parameters and embedded in similarly sized breasts.

3.2. Hybrid simulation framework

Intensity scaling only mimics the contrast based on existing structures. To account for the influence of imaging system properties on virtually imaged lesions, researchers have developed hybrid simulation methods. This allows for a more realistic insertion of a lesion model into an existing projection image of a (pathology-free) patient breast. Several hybrid simulation frameworks have been described (Carton *et al* 2003, Shaheen *et al* 2011, Elangovan *et al* 2014, Vancoillie *et al* 2020) to form hybrid projection images, all using a broadly similar approach (figure 10).

In the first step, a 2D template of the lesion model is generated by calculating the primary x-ray transmission through the 3D lesion for every projection using a ray tracing technique. This accounts for the background composition at the insertion location. The influence of x-ray system factors that influence image sharpness, such as the x-ray focus size and blurring due to the x-ray detector, is then incorporated. To do this, primary templates are multiplied by the system modulation transfer function, which is assumed to characterise these blurring factors. Additionally, the template contrast is modified using a scatter-to-primary ratio relevant to the breast thickness/composition and the energy. Finally, the modified breast lesion template is combined with the background image. Furthermore, a change in signal at the insertion site will affect the background noise wherefore corrections can be applied (Elangovan *et al* 2014).



Carton *et al* (2003) and Zanca *et al* (2008) used these methods to modify initial templates for a range of system parameters. In other work, the hybrid tool developed by Shaheen *et al* (2010) for simulating 3D lesions was validated in depth by Vancoillie *et al* (2020) and applied in a number of studies (Shaheen *et al* 2011, Salvagnini *et al* 2016, Van Camp *et al* 2022). Similarly, Ho *et al* (2010) used the algorithm given by Tromans and Brandy (2010) to model image formation by considering the size and location of the microcalcifications. The study of Näppi *et al* (2001) worked with both real mammographic images and generated backgrounds. The simulation framework created high spatial resolution images using a recursive 2D midpoint displacement algorithm. When simulating the lesion in these background images, the penetration of the x-rays through the 3D calcification was first modelled. Attenuation was then added based on the attenuation derived from the background with a control on the contrast.

3.3. Total simulation framework

A number of groups have developed total simulation frameworks (Bliznakova *et al* 2012, Milioni De Carvalho 2014, Elangovan *et al* 2016a, Barufaldi *et al* 2018, Badal *et al* 2021), in which lesion models are inserted into computationally generated breast phantoms. Breast model simulation is not covered in this paper; therefore we refer to Bliznakova (2020). To simulate cancer cases with a realistic appearance, breast phantoms should be sufficiently detailed next to realistic lesion models.

The most common approach when embedding simulated lesions in a breast model is to replace the background tissue voxels with the corresponding material of the particular pathology. Voxel replacement works efficiently for calcification insertion because its attenuation is markedly higher than that of healthy breast tissue. However, for mass lesions, the replacement method cannot guarantee that their x-ray attenuation properties will be adequately simulated, and can consequently bias detection studies (Barufaldi *et al* 2022). Barufaldi *et al* (2022) proposed a second approach called voxel addition, which considers the underlying tissue by allowing lesion voxels in the phantom to be composed of an admixture of lesion and breast tissue. Instead of assigning the same attenuation coefficients to all voxels of the mass lesion, Bliznakova *et al* (2019) introduced smooth integration by changing the properties of the lesion in proportion to the distance from the lesion centre.

After integration of the lesions within the breast model, image acquisition can be simulated using different methods, such as Monte Carlo x-ray transport code or ray tracing, to obtain mammographic images (figure 11). There is also the possibility to perform ray tracing of the lesion and breast phantom separately so that high resolution lesions could be inserted (Elangovan *et al* 2014).

3.4. Use of artificial intelligence

The previously discussed approaches separately develop a lesion model and a breast phantom, followed by insertion of the lesion into this breast phantom or a breast image. Instead, techniques exist that grow or generate lesions directly in breast images to create a cancer case.

Currently, there is an enormous focus on deep learning techniques in medical imaging research (Yi *et al* 2019, Jairam and Ha 2022, Xun *et al* 2022). These methods have also been used to generate synthetic data. Generative adversarial networks (GANs) are particularly suited for data augmentation to aid deep learning networks in lesion detection and classification.

Figure 12 illustrates the basic working principles of a GAN. GANs usually start from noise fed to the generator, which produces output ROIs containing synthetic lesions (Goodfellow *et al* 2014). A discriminator

Figure 11. Outline of the general workflow of a total simulation framework (Images from: github.com/DIDSR/VICTRE).

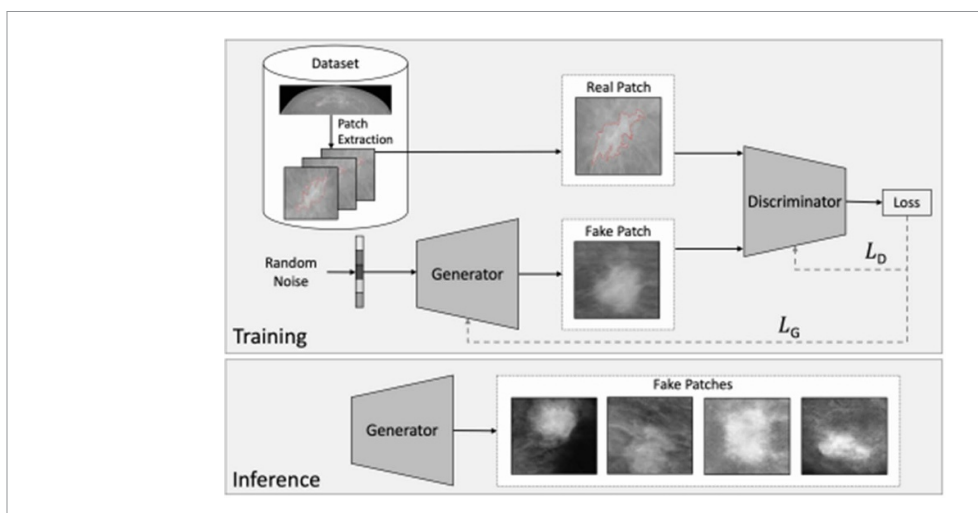


Figure 12. The training and inference steps of a GAN model to generate patches with breast lesions. During training, the generator learns to create realistic patches that can fool the discriminator. For inference, fake patches are then created by the generator. Reproduced with permission from (Szafranowska *et al* 2022).

is then trained concurrently to distinguish between the ROIs with real lesions and the generated ROIs. By adversarial training of both in parallel, the generator will eventually generate realistic ROIs that cannot be distinguished from real tissue by the discriminator. Generation of lesions from an initial noise field is one of the many data augmentation methods that may lead to improvements in breast cancer detection models (Alyafi *et al* 2019b, Guan and Loew 2019, Szafranowska *et al* 2022).

Other work in this area have focused on the translation of normal tissue patches to patches containing a lesion or, alternatively, to remove or make lesions more subtle in an image. Wu et al (2018) and Lee et al (2019) applied conditional GANs in which a classification outcome or BI-RADS description desired for the output image was fed to the generator, in addition to the input image. Wu et al (2020) used a contextual network in which a lesion was generated from a normal breast tissue patch. The generated lesion was subsequently added to the original image. The model was trained to either generate masses or calcifications, or to remove lesions. When defining the location of the lesion, Swieciki et al (2021) removed a square region from the tissue patch. The aim of the generator was to reconstruct this removed region by in-painting a lesion. Shen et al (2021) extended this by first defining a segmentation contour and then training the GAN such that a lesion was generated in the ROI that matched the contour. Some models can synthesise complete mammographic images. Korkinof et al (2018) developed a network in which the resolution was progressively increased. In the first stages, a global breast shape was developed, after which other structures, such as calcifications, appeared in the later stages.

There are several ways in which these synthetic images of breast abnormalities are evaluated: by comparing the spiculation and the circularity of real and simulated masses (Lee *et al* 2019), in terms of improvement of the performance of a classification or detection network (Samala *et al* 2016, Alyafi *et al* 2019a, Guan and Loew 2019), by using relevant quantitative and qualitative image analysis metrics (Oyelade *et al* 2022), or by performing a reader study with real and synthetic image pairs (Korkinof *et al* 2021). Although GANs perform synthesis rather than simulation (Frangi *et al* 2018), mammographic images

generated by deep learning models may prove an important source for VCTs in the future. Their ability to readily generate large sets of data with complex characteristics and realistic insertion into the background tissue can be an advantage. On the other hand, mostly no ground truth is known for GAN-generated lesions, and it provides limited control to the user regarding the physical properties of the lesion or the acquisition system. The fact that GAN models often require a large dataset themselves for training can also be considered a drawback. In medical imaging, such datasets are often limited due to e.g. privacy concerns or the lack of available annotations. With limited data available, a GAN model might fail to converge or, on the other hand, might overfit the training data. This would lead to the creation of lesions that all have a similar appearance which do not cover the versatility of all lesions occurring in mammographic images. Especially when one wants to create rare types of lesions or lesions that are hard to detect, the amount of input data may be too scarce for successful simulation.

3.5. Simulation parameters

3.5.1. Material composition of lesions

A number of studies have examined the materials used to simulate microcalcifications, all expressing microcalcification attenuation properties as equivalent aluminium thickness (Carton *et al* 2004, Zanca *et al* 2010, Warren *et al* 2013). This relationship was later used by Van Camp *et al* (2022). Warren *et al* (2013) also compared the attenuation of CaOx and CaHa and found that microcalcifications could be modelled in VCTs using the attenuation coefficient of solid CaOx, weighted by a factor of 0.84. Other studies have differentiated between calcifications of type I (CaOx) and type II (CaHa) (Daul *et al* 2005, Plourde *et al* 2016, Ghammraoui and Glick 2017, Makeev *et al* 2021). Shaheen *et al* (2011) and Salvagnini *et al* (2016) used CaOx, whereas Bliznakova *et al* (2006) used CaCO₃ as a material to simulate calcifications.

For mass lesions, attenuation coefficients can be assumed to be identical to those of glandular tissue (Chen *et al* 2010). In addition, a multiplication factor of 1.02 (Badano *et al* 2018) or 1.04 (Bakic *et al* 2018a) can be applied to the glandular tissue attenuation coefficient to slightly increase lesion attenuation.

In many studies, lesions are considered to consist of uniform material. Shaheen *et al* (2011) mentioned the limitation of choosing a single material to model microcalcification clusters whereas in reality, this might be a mix of materials and as well differ between calcifications. Apart from this, the deviation in density can be modelled by concentric rings (Lado *et al* 1997, Carton *et al* 2003, Lago *et al* 2018, Bakic *et al* 2018b) or by creating adjusted templates in the simulation process. Sánchez De La Rosa (2019) simulated heterogeneous enhancement patterns inside mass lesions for the investigation of contrast-enhanced mammography.

3.5.2. Insertion location

The insertion location depends strongly on the application. Clearly, lesion location influences observer detection rates in detection studies, depending on the contrast of the local breast structures. When working with image patches, lesions are often inserted at random locations (Warren *et al* 2013, Vivona *et al* 2014, Lago *et al* 2018) with some additional restrictions regarding the distance to the skin and the height in the compressed breast (Mackenzie *et al* 2022). A number of studies have simulated many lesions across a grid in an image to generate an ensemble of detection rates for a given breast background (Bakic *et al* 2018a, Makeev *et al* 2021, Barufaldi *et al* 2022).

In studies showing complete breasts to the observers, the insertion site is often selected manually, as prior knowledge increases the realism of the insertion location. Rashidnasab *et al* (2013b) used the geographical distribution of real screen-detected breast cancers to aid in the selection of locations. Shaheen *et al* (2014) limited the insertion positions to within 80% of the central portion of the breast away from the skin edge. Lapuebla-Ferri *et al* (2017) found the position of the real mass present in the contralateral breast and embedded the simulated lesion in a similar location in the current breast. Suryanarayanan *et al* (2005) selected a location in the vicinity of an existing calcification cluster with intensities in the same range. In addition, radiologist feedback can be used to decide on realistic insertion sites (Rashidnasab *et al* 2013b, Mackenzie *et al* 2022). In order to automate region selection in clinical mammograms, Berks *et al* (2010) constructed a probabilistic model of mass locations from a training set of mammograms that contained annotated masses.

When breast phantoms are generated using the VICTRE *in silico* imaging pipeline, a list of candidate insertion locations is provided. Each location is located close to a terminal duct lobular unit, as this is a common site for cancer formation (Badano *et al* 2018).

3.5.3. Deformation

Very few studies have been reported in the literature on the deformation of breast lesions. For example, breast compression may change the shape of mass lesions. It is well known that malignant breast lesions are generally stiffer than normal breast tissue (Chen *et al* 2019). In most of the simulation pipelines, the breast

phantoms are compressed prior to the insertion of the breast lesion. Deformation is not a concern for microcalcifications because of their small size and high density.

3.5.4. Resolution

Voxelised breast phantoms and mass models have a particular resolution. High-detailed phantoms are necessary for high-resolution imaging applications such as mammography and tomosynthesis. For mathematical models, the chosen resolution is mostly a balance between the required details and simulation efficiency. For models based on segmented imaging data, the presence of small details is determined by the characteristics of the imaging modalities from which the lesions are segmented (e.g. noise, resolution, and contrast) and the segmentation algorithms.

Next, the details of the simulated breast models can be limited by the image simulation pipeline. Some frameworks allow inserting high-resolution models in a breast phantom or in breast images with a lower resolution (Elangovan *et al* 2014, Vancoillie *et al* 2020), while in other frameworks the lesion models are forced to have the same resolution as the background breast structure (Barufaldi *et al* 2018, Badal *et al* 2021). For microcalcifications, a limited resolution may imply that they are modelled as just a single cubic voxel. For the mass models, it is mainly the spicules that suffer from low resolution. On the other hand, the partial volume effect should be considered. When both lesion and background material occur in the same voxel, errors may arise in simulating the correct size of small structures. Therefore, appropriate voxel computations such as addition or multiplication rather than voxel replacement allow the smooth blending or integration of the lesion in the surrounding tissue.

4. Applications

Tumour models are often used in detectability studies, where the image interpretation is performed by human observers using the *m*-alternative forced choice paradigm (Burgess 1995, 1999) or by computational readers. The detectability of a lesion in the breast using x-ray imaging can be affected by many factors, including image acquisition methods, radiation dose, image processing, reconstruction algorithms, physical properties of the breast, and the lesion itself. To optimise x-ray breast imaging systems, simulated lesions can be used to investigate the effects of different imaging conditions on cancer detection.

Previous investigations included the effect of compressed breast thickness on lesion detectability in DM (Salvagnini *et al* 2016); the effect of tomographic scan angular range and number of projections on microcalcification and mass detection (Sechopoulos and Ghetti 2009, Hadjipanteli *et al* 2017, 2019); the radiation dose dependence of mass and microcalcification detection (Ruschin *et al* 2007, Hadjipanteli *et al* 2017); the impact of different detectors, dose levels, and different image processing algorithms on microcalcification detection (Zanca *et al* 2009, Warren *et al* 2012); the effect of quantum noise on lesion detectability (Reiser and Nishikawa 2010); the detection accuracy for breast masses and microcalcification clusters with a variable dose acquisition technique (Das *et al* 2009); and the masking effect of simulated masses by densities on detectability (Mainprize *et al* 2016).

Simulated lesions can also be used to compare imaging modalities, with a comparison of lesion detectability in DM versus DBT being a frequently studied research question (Timberg *et al* 2010, Shaheen *et al* 2011, Hadjipanteli *et al* 2017, Badano *et al* 2018, Elangovan *et al* 2018, Bakic *et al* 2018a). The benefits of dual-energy systems have been studied (Bliznakova *et al* 2003) as well as the use of breast CT imaging in comparison with DM and DBT (Gong *et al* 2006). The detection thresholds using spherical targets in such studies may not apply to more complex masses, such as irregular target shapes (Elangovan *et al* 2018). Consequently, these results have reduced relevance compared to clinical diagnostic tasks.

Outside detection tasks, simulated lesions can be used to investigate diagnostic tasks performed by radiologists under specific imaging conditions. Reiser and Nishikawa (2006) investigated the human performance in discriminating between differently shaped simulated microcalcifications. Lesion models can also be used in observer trials of visual search models, for example, in terms of signal detectability of simulated microcalcifications and masses in single 2D and 3D images (Lago *et al* 2018, 2018).

Another application for synthetically generated images with simulated lesions is to evaluate the performance of algorithms and software, such as morphological enhancement algorithms applied to microcalcifications (Jagannath *et al* 2012), clustering models for microcalcifications (Vivona *et al* 2014), or computer-aided detection systems (Makeev *et al* 2021). Deep learning models can be evaluated or trained (Guan and Loew 2019, Szafranowska *et al* 2022), just as radiologists can learn from synthetic images (Näppi *et al* 2001).

Depending on the research question, a suitable breast lesion model is chosen. Currently, the largest application of lesion models in VCTs concerns detectability studies to quantify system performance under different imaging conditions. Most of the lesion models used in detection studies are based on mathematical

methods. Fewer VCT applications have been found that use simulated lesions to investigate diagnostic performance, as this may require more realistic lesion models. Mass models based on patient data have not yet found their way to the applications. The increasing acceptance of VCTs in medical imaging by researchers, as well as by industry and government, has advanced the use of VCTs in regulatory approval (Barufaldi *et al* 2021). In addition, these studies can be instrumental in prototyping clinical trials.

5. Summary

In this review, a wide range of methods for generating and simulating breast lesion models is discussed. Most of these methods for both microcalcification clusters and masses are based on either mathematical models or on patient data. The former has the advantage that a more automated method to generate lesions is available, whereas the latter approach generates lesions with a high level of realism at the expense of flexibility. Although simple models are useful for detectability studies, introducing a higher level of complexity in lesion models opens up a broader range of applications.

These lesions are embedded in patient images or virtual breast phantoms. Intensity scaling can be applied to adjust the contrast of lesion models embedded in breast structure. On the other hand, hybrid and total simulation frameworks encompass more parameters in order to simulate the imaging systems used for mammographic acquisition. In addition to simulating the lesion attenuation, they also consider correct insertion into the surrounding tissue using, for example, voxel replacement or addition. Recently, deep learning-based methods have approached the simulation of breast lesions from a different angle by directly growing the lesion in existing breast tissue with the use of GANs. Unlike the conventional generation of lesion models, they face the difficulty of specifying features and types, and of explicitly incorporating system imaging characteristics.

With the wide range of generation and simulation methods, the applications covered also vary. While detectability studies and diagnostic performance studies can be performed, for example, to compare imaging modalities, synthetic data can also be used to evaluate and train software and algorithms.

Despite the evolution towards more detailed and complex lesion models and the development of different simulation platforms to incorporate these lesions into background structures, there are still many challenges for the future. A major challenge for VCT design is the selection of appropriate lesion characteristics so that the results obtained match or predict performance in clinical practice. Notwithstanding the progress made regarding the realism of breast lesion models, further steps must be taken. As the realism of simulated lesions increases, so does the relevance and predictive power of virtual studies with respect to different patient populations. This will also allow models and applications to be more readily applied in clinical practice. Badano (2017) stated that realism may not be considered the first approximation for assessing *in silico* imaging methods. VCTs must be assessed based on their purpose. The ability to distinguish between real and simulated images may not be relevant for the value of VCTs in evaluating imaging system innovations.

Challenges in the simulation process include determining realistic insertion locations in the breast with respect to lesion characteristics. For example, linear calcifications are only located in the ducts. Depending on the lesion type and insertion position, the absence of associated features, such as skin retraction and architectural distortions, limits the realism and may influence the decision of the radiologist in a validation study. Another challenge, particularly when using the hybrid simulation approach, is to ensure that the lesion blends correctly with the background structures. The realism of the lesion models cannot be studied in isolation, as the resulting images are the product of the entire simulation framework. This emphasises the importance of thorough validation of the simulation pipeline and introduces a challenge on the objective validation of lesion models.

In future work, a challenge to be faced is the ability to create an extensive dataset that includes the full variety of lesions occurring in the patient population, including both benign and malignant lesions, small subtle lesions but also extensive tumours, all different subtypes including both common and rare types, etc. If VCT results are to be predictive of real clinical studies or trials, all of these aspects and related simulation steps must be incorporated. The key concern is the accuracy of the simulated images in terms of figures of merit that are meaningful for the intended task.

Data availability statement

No new data were created or analysed in this study.

Acknowledgments

Authors acknowledge the global partnership agreement 2020 KU Leuven—Maastricht University. Authors acknowledge financial support from the European Union's Horizon 2020 research and innovation program under Grant Agreement: CHAIMELEON n° 952172, EuCanImage n° 952103 and IMI-OPTIMA n° 101034347.

ORCID iDs

Astrid Van Camp © https://orcid.org/0000-0001-5007-9755 Katrien Houbrechts © https://orcid.org/0000-0002-2862-3504 Nicholas W Marshall © https://orcid.org/0000-0001-5549-5133

References

Abadi E, Segars W P, Tsui B M W, Kinahan P E, Bottenus N, Frangi A F, Maidment A, Lo J and Samei E 2020 Virtual clinical trials in medical imaging: a review *J. Med. Imaging* 7 042805

Alyafi B et al 2019a Quality analysis of DCGAN-generated mammography lesions IWBI 2020: Proc. 15th Int. Workshop on Breast Imaging p 115130B

Alyafi B, Diaz O and Marti R 2019b DCGANs for realistic breast mass augmentation in x-ray mammography *Proc. SPIE* 11314 1131420 American College of Radiology 2013 ACR BI-RADS® Atlas, Breast Imaging Reporting and Data System (Reston, VA)

Badal A, Sharma D, Graff C G, Zeng R and Badano A 2021 Mammography and breast tomosynthesis simulator for virtual clinical trials Comput. Phys. Commun. 261 107779

Badano A 2017 "How much realism is needed?"—the wrong question *in silico* imagers have been asking *Med. Phys.* 44 1607–9
Badano A, Graff C G, Badal A, Sharma D, Zeng R, Samuelson F W, Glick S J and Myers K J 2018 Evaluation of digital breast tomosynthesis as replacement of full-field digital mammography using an *in silico* imaging trial *JAMA Netw. Open* 1 e185474

Bakic P R *et al* 2018a Virtual clinical trial of lesion detection in digital mammography and digital breast tomosynthesis *Proc. SPIE* **10573** 1057306

Bakic P R et al 2018b Optimized simulation of breast anatomy for virtual clinical trials *IWBI 2018*: Proc. 14th Int. Workshop on Breast Imaging p 107181X

Barufaldi B et al 2018 OpenVCT: a GPU-accelerated virtual clinical trial pipeline for mammography and digital breast tomosynthesis Proc. SPIE 10573 1057358

Barufaldi B, Maidment A D A, Dustler M, Axelsson R, Tomic H, Zackrisson S, Tingberg A and Bakic P R 2021 Virtual clinical trials in medical imaging system evaluation and optimisation *Radiat. Prot. Dosim.* 195 363–71

Barufaldi B, Vent T L, Bakic P R and Maidment A D A 2022 Computer simulations of case difficulty in digital breast tomosynthesis using virtual clinical trials *Med. Phys.* 49 2220–32

Bent C K, Bassett L W, D'Orsi C J and Sayre J W 2010 The positive predictive value of BI-RADS microcalcification descriptors and final assessment categories Am. J. Roentgenol. 194 1378–83

Berks M et al 2008 Statistical appearance models of mammographic masses IWDM 2008: Proc. 9th Int. Workshop on Digital Mammography pp 401–8

 $Berks\ M\ et\ al\ 2010\ Synthesising\ malignant\ breast\ masses\ in\ normal\ mammograms\ \textit{Lect. Notes}\ \textit{Comput. Sci.}\ \textbf{6136}\ 505-12$

Berks M and Barbosa da Silva D 2010 Evaluating the realism of synthetically generated mammographic lesions: an observer study *Proc.* SPIE 7627 762704

Bliznakova K et al 2019 Development of breast lesions models database Phys. Medica 64 293-303

Bliznakova K 2020 The advent of anthropomorphic three-dimensional breast phantoms for x-ray imaging Phys. Medica 79 145–61Bliznakova K, Bliznakov Z, Bravou V, Kolitsi Z and Pallikarakis N 2003 A three-dimensional breast software phantom for mammography simulation Phys. Med. Biol. 48 3699–719

Bliznakova K, Kolitsi Z and Pallikarakis N 2006 Dual-energy mammography: simulation studies Phys. Med. Biol. 51 4497-515

Bliznakova K, Sechopoulos I, Buliev I and Pallikarakis N 2012 BreastSimulator: a software platform for breast x-ray imaging research *J. Biomed. Graph. Comput.* 2 1

Burgess A E 1995 Comparison of receiver operating characteristic and forced choice observer performance measurement methods *Med. Phys.* 22 643–55

Burgess A E 1999 Mammographic structure: data preparation and spatial statistics analysis Proc. SPIE 3661 642-53

Burnside E S, Ochsner J E, Fowler K J, Fine J P, Salkowski L R, Rubin D L and Sisney G A 2007 Use of microcalcification descriptors in BI-RADS 4th edition to stratify risk of malignancy *Radiology* 242 388–95

Carton A-K, Bosmans H, Van Ongeval C, Souverijns G, Rogge F, Van Steen A and Marchal G 2003 Development and validation of a simulation procedure to study the visibility of micro calcifications in digital mammograms Med. Phys. 30 2234–40

Carton A-K, Bosmans H, Vandenbroucke D, Souverijns G, Van Ongeval C, Dragusin O and Marchal G 2004 Quantification of Al-equivalent thickness of just visible microcalcifications in full field digital mammograms *Med. Phys.* 31 2165–76

Chan H-P, Sahiner B, Lam K L, Petrick N, Helvie M A, Goodsitt M M and Adler D D 1998 Computerized analysis of mammographic microcalcifications in morphological and texture feature spaces *Med. Phys.* 25 2007–19

Chen B, Shorey J, Saunders R S, Richard S, Thompson J, Nolte L W and Samei E 2011 An anthropomorphic breast model for breast imaging simulation and optimization *Acad. Radiol.* 18 536–46

Chen J-H, Chan S, Zhang Y, Li S, Chang R-F and Su M-Y 2019 Evaluation of breast stiffness measured by ultrasound and breast density measured by MRI using a prone-supine deformation model *Biomark*. Res. 7 1–10

Chen R C et al 2010 Measurement of the linear attenuation coefficients of breast tissues by synchrotron radiation computed tomography Phys. Med. Biol. 55 4993–5005

D'Orsi C J and Kopans D B 1993 Mammographic feature analysis Semin. Roentgenol. 28 204–30

Das M, Gifford H C, O'connor J M and Glick S J 2009 Evaluation of a variable dose acquisition technique for microcalcification and mass detection in digital breast tomosynthesis *Med. Phys.* 36 1976–84

- Daul C, Graebling P, Tiedeu A and Wolf D 2005 3D reconstruction of microcalcification clusters using stereo imaging: algorithm and mammographic unit calibration *IEEE Trans. Biomed. Eng.* 52 2058–73
- De Sisternes L, Brankov J G, Zysk A M, Schmidt R A, Nishikawa R M and Wernick M N 2015 A computational model to generate simulated three-dimensional breast masses *Med. Phys.* 42 1098–118
- duCret R P 1997 Mammographic interpretation: a practical approach. 2nd ed Radiology 204 480
- Dukov N, Bliznakova K, Feradov F, Buliev I, Bosmans H, Mettivier G, Russo P, Cockmartin L and Bliznakov Z 2019 Models of breast lesions based on three-dimensional x-ray breast images *Phys. Medica* 57 80–87
- Elangovan P et al 2016a OPTIMAM image simulation toolbox—recent developments and ongoing studies IWDM 2016: 13th Int. Workshop on Breast Imaging pp 668–75
- Elangovan P et al 2016b Simulation of spiculated breast lesions Proc. SPIE 9783 97832E
- Elangovan P, Mackenzie A, Dance D R, Young K C and Wells K 2018 Lesion detectability in 2D-mammography and digital breast tomosynthesis using different targets and observers Phys. Med. Biol. 63 095014
- Elangovan P, Warren L M, Mackenzie A, Rashidnasab A, Diaz O, Dance D R, Young K C, Bosmans H, Strudley C J and Wells K 2014 Development and validation of a modelling framework for simulating 2D-mammography and breast tomosynthesis images *Phys. Med. Biol.* 59 4275–93
- Frangi A F, Tsaftaris S A and Prince J L 2018 Simulation and synthesis in medical imaging IEEE Trans. Med. Imaging 37 673-9
- Gaur S, Dialani V, Slanetz P J and Eisenberg R L 2013 Architectural distortion of the breast Am. J. Roentgenol. 201 662-70
- Ghammraoui B and Glick S J 2017 Investigating the feasibility of classifying breast microcalcifications using photon-counting spectral mammography: a simulation study *Med. Phys.* 44 2304–11
- Gong X, Glick S J, Liu B, Vedula A A and Thacker S 2006 A computer simulation study comparing lesion detection accuracy with digital mammography, breast tomosynthesis, and cone-beam CT breast imaging Med. Phys. 33 1041–52
- Goodfellow I et al 2014 Generative adversarial networks Advances in Neural Information Processing Systems vol 27 pp 2672-80
- Guan S and Loew M 2019 Breast cancer detection using synthetic mammograms from generative adversarial networks in convolutional neural networks *J. Med. Imaging* 6 031411
- Hadjipanteli A, Elangovan P, Mackenzie A, Looney P T, Wells K, Dance D R and Young K C 2017 The effect of system geometry and dose on the threshold detectable calcification diameter in 2D-mammography and digital breast tomosynthesis *Phys. Med. Biol.* 62 858–77
- Hadjipanteli A, Elangovan P, Mackenzie A, Wells K, Dance D R and Young K C 2019 The threshold detectable mass diameter for 2D-mammography and digital breast tomosynthesis *Phys. Medica* 57 25–32
- Hintsala H et al 2009 Modelling of irregular breast lesions World Congress on Medical Physics and Biomedical Engineering: IFMBE Proc. vol 25 pp 2024–7
- Ho C P S et al 2010 Classification of clusters of microcalcifications in digital breast tomosynthesis Annual Int. Conf. IEEE Engineering in Medicine and Biology Society 2010 pp 3166–9
- Jagannath H S, Virmani J and Kumar V 2012 Morphological enhancement of microcalcifications in digital mammograms J. Inst. Eng. Electr. Eng. B 93 163–72
- Jairam M P and Ha R 2022 A review of artificial intelligence in mammography Clin. Imaging 88 36-44
- Kallergi M, Gavrielides M A, Li H, Berman C G, Kim J J and Clark R A 1998 Simulation model of mammographic calcifications based on the American College of Radiology Breast Imaging Reporting and Data System, or BIRADS *Acad. Radiol.* 5 670–9
- Korkinof D et al 2018 High-resolution mammogram synthesis using progressive generative adversarial networks (arXiv:1807.03401)
- Korkinof D, Harvey H, Heindl A, Karpati E, Williams G, Rijken T, Kecskemethy P and Glocker B 2021 Perceived realism of high-resolution generative adversarial network–derived synthetic mammograms *Radiol. Artif. Intell.* 3 e190181
- Lado M J, Tahoces P G, Souto M, Méndez A J and Vidal J J 1997 Real and simulated clustered microcalcifications in digital mammograms. ROC study of observer performance Med. Phys. 24 1385–94
- Lago M A et al 2018 Interactions of lesion detectability and size across single-slice DBT and 3D DBT Proc. SPIE 10577 105770X
- Lago M A, Eckstein M P and Abbey C K 2018 Evaluation of search strategies for microcalcifications and masses in 3D images *Proc. SPIE* **10577** 105770C
- Lapuebla-Ferri A, Cegoñino-Banzo J, Jiménez-Mocholí A-J and Del Palomar A P 2017 Towards an in-plane methodology to track breast lesions using mammograms and patient-specific finite-element simulations *Phys. Med. Biol.* **62** 8720–38
- Le Gal M, Chavanne G and Pellier D 1984 Diagnostic value of clustered microcalcifications discovered by mammography (apropos of 227 cases with histopathological verification and without a palpable breast tumor) *Bull. Cancer* **71** 57–64
- Lee H et al 2019 Realistic breast mass generation through BIRADS category MICCAI 2019: Medical Image Computing and Computer Assisted Intervention vol 11769 pp 703–11
- Li Z et al 2018 Comparison of microcalcification detectability in FFDM and DBT using a virtual clinical trial *Proc. SPIE* 10577 105770D Mackenzie A et al 2022 Virtual clinical trial to compare cancer detection using combinations of 2D mammography, digital breast tomosynthesis and synthetic 2D imaging *Eur. Radiol.* 32 806–14
- Mainprize J G, Alonzo-Proulx O, Jong R A and Yaffe M J 2016 Quantifying masking in clinical mammograms via local detectability of simulated lesions *Med. Phys.* 43 1249–58
- Makeev A, Rodal G, Ghammraoui B, Badal A and Glick S J 2021 Exploring CNN potential in discriminating benign and malignant
- calcifications in conventional and dual-energy FFDM: simulations and experimental observations *J. Med. Imaging* 8 1–16 Marshall N W and Bosmans H 2022 Performance evaluation of digital breast tomosynthesis systems: comparison of current virtual clinical trial methods *Phys. Med. Biol.* 67 22TR04
- Milioni De Carvalho P 2014 Low-dose 3D quantitative vascular x-ray imaging of the breast *PhD Dissertation* Paris-Sud University (available at: https://theses.hal.science/tel-01292379/file/VD2_MILIONI-DE-CARVALHO_PABLO_22092014.pdf)
- Näppi J, Dean P B, Nevalainen O and Toikkanen S 2001 Algorithmic 3D simulation of breast calcifications for digital mammography Comput. Methods Programs Biomed. 66 115–24
- Oyelade O N, Ezugwu A E, Almutairi M S, Saha A K, Abualigah L and Chiroma H 2022 A generative adversarial network for synthetization of regions of interest based on digital mammograms Sci. Rep. 12 6166
- Plourde S M, Marin Z, Smith Z R, Toner B C, Batchelder K A and Khalil A 2016 Computational growth model of breast microcalcification clusters in simulated mammographic environments *Comput. Biol. Med.* 76 7–13
- Rashidnasab A et al 2013a Simulation of 3D DLA masses in digital breast tomosynthesis Proc. SPIE 8668 86680Y
- Rashidnasab A, Elangovan P, Yip M, Diaz O, Dance D R, Young K C and Wells K 2013b Simulation and assessment of realistic breast lesions using fractal growth models *Phys. Med. Biol.* **58** 5613–27

- Reiser I and Nishikawa R M 2006 Identification of simulated microcalcifications in white noise and mammographic backgrounds Med. Phys. 33 2905–11
- Reiser I and Nishikawa R M 2010 Task-based assessment of breast tomosynthesis: effect of acquisition parameters and quantum noise Med. Phys. 37 1591–600
- Ruschin M et al 2007 Dose dependence of mass and microcalcification detection in digital mammography: free response human observer studies Med. Phys. 34 400–7
- Ruschin M, Tingberg A, Båth M, Grahn A, Håkansson M, Hemdal B and Andersson I 2005 Using simple mathematical functions to simulate pathological structures—input for digital mammography clinical trial *Radiat. Prot. Dosim.* 114 424–31
- Salvagnini E, Bosmans H, Van Ongeval C, Van Steen A, Michielsen K, Cockmartin L, Struelens L and Marshall N W 2016 Impact of compressed breast thickness and dose on lesion detectability in digital mammography: FROC study with simulated lesions in real mammograms Med. Phys. 43 5104–16
- Samala R K, Chan H-P, Hadjiiski L, Helvie M A, Wei J and Cha K 2016 Mass detection in digital breast tomosynthesis: deep convolutional neural network with transfer learning from mammography *Med. Phys.* 43 6654–66
- Sánchez De La Rosa R 2019 Simulations and virtual clinical trials for the assessment of the added clinical value of angio-tomosynthesis over angio-mammography *PhD Dissertation* Paris-Saclay University (available at: www.theses.fr/2019SACLT046.pdf)
- Saunders R, Samei E, Baker J and Delong D 2006 Simulation of mammographic lesions Acad. Radiol. 13 860-70
- Sechopoulos I and Ghetti C 2009 Optimization of the acquisition geometry in digital tomosynthesis of the breast *Med. Phys.* **36** 1199–207 Sengupta A, Sharma D and Badano A 2021 Computational model of tumor growth for *in silico* trials *Proc. SPIE* **11595** 115954S
- Shaheen E, De Keyzer F, Bosmans H, Dance D R, Young K C and Ongeval C V 2014 The simulation of 3D mass models in 2D digital mammography and breast tomosynthesis *Med. Phys.* 41 081913
- Shaheen E, Van Ongeval C, Zanca F, Cockmartin L, Marshall N, Jacobs J, Young K C, R Dance D and Bosmans H 2011 The simulation of 3D microcalcification clusters in 2D digital mammography and breast tomosynthesis Med. Phys. 38 6659–71
- Shaheen E, Zanca F, Sisini F, Zhang G, Jacobs J and Bosmans H 2010 Simulation of 3D objects into breast tomosynthesis images *Radiat. Prot. Dosim.* 139 108–12
- Shen T, Hao K, Gou C and Wang F-Y 2021 Mass image synthesis in mammogram with contextual information based on GANs Comput. Methods Programs Biomed. 202 106019
- Suryanarayanan S, Karellas A, Vedantham S, Waldrop S M and D'Orsi C J 2005 Detection of simulated lesions on data-compressed digital mammograms Radiology 236 31–36
- Swiecicki A, Konz N, Buda M and Mazurowski M A 2021 A generative adversarial network-based abnormality detection using only normal images for model training with application to digital breast tomosynthesis Sci. Rep. 11 1–13
- Szafranowska Z et al 2022 Sharing generative models instead of private data: a simulation study on mammography patch classification (arXiv:2203.04961)
- Tiedeu A, Daul C, Graebling P and Wolf D 2005 Correspondences between microcalcification projections on two mammographic views acquired with digital systems Comput. Med. Imaging Graph. 29 543–53
- Timberg P, Båth M, Andersson I, Mattsson S, Tingberg A and Ruschin M 2010 In-plane visibility of lesions using breast tomosynthesis and digital mammography *Med. Phys.* 37 5618–26
- Tomic H et al 2021 Assessment of a tumour growth model for virtual clinical trials of breast cancer screening Proc. SPIE 11595 115954Q
 Tromans C E and Brady M 2010 The standard attenuation rate for quantitative mammography Lecture Notes in Computer Science
 (including subseries Lecture Notes in Artificial Intelligence and Lecture Notes in Bioinformatics vol 6136) pp 561–8
- Van Camp A *et al* 2022 The creation of a large set of realistic synthetic microcalcification clusters for simulation in (contrast-enhanced) mammography images *Proc. SPIE* 12031 120310V
- Vancoillie L, Marshall N, Cockmartin L, Vignero J, Zhang G and Bosmans H 2020 Verification of the accuracy of a hybrid breast imaging simulation framework for virtual clinical trial applications *J. Med. Imaging* 7 042804
- Vivona L, Cascio D, Fauci F and Raso G 2014 Fuzzy technique for microcalcifications clustering in digital mammograms *BMC Med. Imaging* 14 1–18
- Warren L M, Mackenzie A, Cooke J, Given-Wilson R M, Wallis M G, Chakraborty D P, Dance D R, Bosmans H and Young K C 2012 Effect of image quality on calcification detection in digital mammography *Med. Phys.* 39 3202–13
- Warren L M, Mackenzie A, Dance D R and Young K C 2013 Comparison of the x-ray attenuation properties of breast calcifications, aluminium, hydroxyapatite and calcium oxalate *Phys. Med. Biol.* 58 N103–13
- Wu E et al 2018 Conditional infilling GANs for data augmentation in mammogram classification Lecture Notes in Computer Science: Image Analysis for Moving Organ, Breast, and Thoracic Images p 11040
- Wu E, Wu K and Lotter W 2020 Synthesizing lesions using contextual GANs improves breast cancer classification on mammograms (arXiv:2006.00086)
- Xun S et al 2022 Generative adversarial networks in medical image segmentation: a review Comput. Biol. Med. 140 105063
- Yam M, Brady M, Highnam R, Behrenbruch C, English R and Kita Y 2001 Three-dimensional reconstruction of microcalcification clusters from two mammographic views *IEEE Trans. Med. Imaging* 20 479–89
- Yi X, Walia E and Babyn P 2019 Generative adversarial network in medical imaging: a review Med. Image Anal. 58 101552
- Zanca F, Chakraborty D P, Van Ongeval C, Jacobs J, Claus F, Marchal G and Bosmans H 2008 An improved method for simulating microcalcifications in digital mammograms *Med. Phys.* 35 4012–8
- Zanca F, Jacobs J, Van Ongeval C, Claus F, Celis V, Geniets C, Provost V, Pauwels H, Marchal G and Bosmans H 2009 Evaluation of clinical image processing algorithms used in digital mammography *Med. Phys.* 36 765–75
- Zanca F, Van Ongeval C, Marshall N, Meylaers T, Michielsen K, Marchal G and Bosmans H 2010 The relationship between the attenuation properties of breast microcalcifications and aluminum *Phys. Med. Biol.* **55** 1057–68